Journal of The Electrochemical Society, **154** (4) G85-G94 (2007)
0013-4651/2007/154(4)/G85/10/$20.00 © The Electrochemical Society

Pore Sealing by NH_3 Plasma Treatment of Porous Low Dielectric Constant Films

Hua-Gen Peng,[a] Dong-Zhi Chi,[b] Wei-De Wang,[b] Jing-Hui Li,[b] Kai-Yang Zeng,[b,c] Richard S. Vallery,[a] William E. Frieze,[a] Mark A. Skalsey,[a] David W. Gidley,[a] and Albert F. Yee[a,d,z]

[a]*Department of Physics, University of Michigan, Ann Arbor, Michigan 48109, USA*
[b]*Institute of Materials Research and Engineering, Singapore, 117602*
[c]*Department of Mechanical Engineering, National University of Singapore, Singapore, 117576*
[d]*California Institute for Telecommunications and Information Technology, University of California–Irvine, Irvine, California 92697, USA*

Porous interlayer dielectric films with interconnected pores pose a serious challenge for their integration into next-generation microchips. The opening of interconnected pores in the surface region needs to be sealed to prevent intrusion of atomic layer deposition precursors used to create metal diffusion barriers. In this paper, we report the formation of a thin, nonporous surface layer on a porous methyl-silsesquioxane-based dielectric film by NH_3 plasma treatment. Depth-profiled beam positronium annihilation lifetime spectroscopy was applied to conveniently examine the formation of the dense layer. A nonporous surface layer was readily identified by the curtailment of positronium escape into vacuum through the surface. Among plasma treatments at temperatures ranging from 25 to 300°C for duration of 3–600 s, the best result was achieved at 300°C for 10 s. A very thin skin layer, ~10 nm, could be formed with little damage to the bulk of the low-κ film. This thin skin layer further proved to improve the performance of Ta barriers for Cu diffusion. Chemical analysis, infrared spectroscopy, and sputtering secondary ion mass spectroscopy were also performed to examine how the plasma treatment altered the dielectric film.
 [DOI: 10.1149/1.2435625]

Manuscript submitted September 22, 2006; revised manuscript received November 30, 2006.
Available electronically February 12, 2007.

While the semiconductor industry continues to scale down device sizes for better performance, lower power consumption and higher packing density, the interconnect delay and cross-talk between adjacent metal lines must be reduced. The industry achieves these objectives by replacing aluminum with copper to increase the conductivity of metal lines and substituting the conventional SiO_2 with low dielectric constant (κ) materials to reduce the κ of the interlayer dielectrics (ILDs).[1,2] According to the *2005 International Technology Roadmap for Semiconductors (ITRS)*, the current ILDs have a minimum κ of 2.7, which is much lower than that of SiO_2 at about 4.0. This reduction in κ is realized by incorporating carbon and hydrogen into the SiO_2 network through chemical vapor deposition of substituted silanes or siloxanes.[3-5] As the projected κ of the interlayer dielectrics needs to keep on decreasing, pores have to be introduced into the dense dielectric matrix, e.g., by decomposing nanometer-sized labile organic porogen domains co-deposited with the dielectric precursor.[2,3,6-8] However, such pores not only significantly compromise the mechanical and electrical performance of the dielectric, they also render the dielectric vulnerable to further degradation during several steps of the fabrication process, resulting in an increase of the effective κ and even failure of the ILDs.[9-11] These integration challenges have delayed the implementation of porous low-κ materials for years as evidenced by the repeatedly revised projections on the deployment of such materials in previous ITRS publications.

It has been demonstrated that metal barriers on low-κ materials are indispensable to block Cu diffusion into ILDs.[12] Low-κ materials have lower densities and looser bonding network than silica and their vulnerability to metal diffusion is further aggravated by the introduction of pores. According to the 2005 ITRS, one of the important issues facing ILDs is "barrier engineering," which means, among other things, the construction of very thin low resistivity metal barrier layers and efficient sealing of pores in low-κ materials. Pore sealing serves more than one purpose because it not only protects the pores from contaminating chemical species during fabrication, but also offers a dense surface on which a thinner metal barrier layer can be deposited. In recent years, atomic layer deposition (ALD) has been identified as one of the most promising thin film deposition techniques to enable nanoscale device fabrication due to its benefits over other conventional deposition techniques such as physical vapor deposition and chemical vapor deposition (CVD).[13] The advantages include the capability to control thickness at the atomic scale, to produce highly conformal films on very small feature sizes, and to cover wide areas with excellent uniformity.[13,14] With the Cu interconnect technology, Ta-based materials (e.g., Ta and TaN) have been identified as the most suitable materials for diffusion barrier applications.[15] However, the excellent conformality of ALD may elicit special problems for porous low-κ materials because the gaseous ALD precursor is able to diffuse into the dielectric film if there are open pores on the film surface and end up covering the wall of pores in the bulk of the film. In severe cases, TiN has been found to penetrate throughout the entire low-κ layer.[16,17] Therefore, a process step to seal the surface of porous ILDs is urgently needed.

Several pore sealing approaches have been reported in the literature and some of the efforts have been discussed in a recent review.[2] One natural solution is to deposit a layer of material on top of the porous dielectrics to simply fill the pores. For instance, 3-methylsilane was deposited to form a sealing layer either of amorphous hydrogenated SiC by plasma enhanced CVD[18-20] or of silicon oxycarbide by UV ozone.[21] CVD Parylene-N has also been shown to work as a pore sealant for porous low-κ materials but it penetrates significantly into the porous dielectric.[22,23] Besides CVD deposition, an ALD process involving catalytic growth of a thin silica layer in the pores near the surface has demonstrated pore-sealing capability as well.[24] In addition to deposition of new materials on top of the porous film, plasma treatment has also attracted a lot of interest as a means to achieve pore sealing.[25-31] In fact, plasma treatment is already involved in several microchip fabrication processes, such as etching of trenches and vias and stripping of the photoresist. The interaction of plasmas with low-κ dielectrics was reviewed in a recent paper.[2] The versatile plasmas have been demonstrated to alter many properties of dielectrics, such as κ value,[11] moisture uptake,[32,33] and leakage current.[34,35] For porous dielectrics, plasmas may not only modify the properties of the solid material, they can also cause pore collapse and pore filling. In favorable cases, the pore collapse and pore filling are concentrated in the surface region of the dielectric so that pore sealing can be realized.[26,28,29,36,37]

[z] E-mail: afyee@uci.edu

The goal of pore sealing via plasma treatment, as well as via other approaches, is to create a dense, yet thin, surface layer. A thick sealing layer will inevitably result in the increase of the effective κ of ILDs. In the research described in this paper, a NH_3 plasma was applied to create a very thin $\sim$10 nm dense layer on a methylsilsesquioxane (MSQ) porous dielectric. Plasma temperature and exposure duration were tuned to optimize the result. Positronium annihilation lifetime spectroscopy (PALS) was used to verify the formation of a sealing layer. PALS offers a simple, nondestructive, and nonintrusive technique to detect pore collapse and pore sealing.[37] Changes to the film chemistry, enhancement of surface mechanical properties, and improvement of Ta metal barrier performance were observed using secondary ion mass spectroscopy (SIMS), Fourier transform infrared (FTIR), scanning electron microscopy (SEM), and nano-indentation. Considering this range of effects on the dielectric film properties we will find that plasma treatment offers a viable and tunable approach for sealing pores in porous low-κ films.

Experimental

Materials.— Porous MSQ samples (Zirkon LK2200™, $\sim$1 μm on Si) were supplied by Shipley. Pieces of LK 2200 films were cleaved from the same wafer as the pristine film and subject to NH_3 plasma treatment under the following plasma conditions: 150 W power at radio frequency 460 kHz, a NH_3 flow rate of 100 sccm (standard cubic centimeter per minute), and gas pressure at 0.3 Torr. Extensive plasma treatments at 300°C substrate temperature for various times (3, 10, 30, 60, and 600 s) were performed. Treatments at 25, 100, and 200°C were also done for comparisons. To study the performance of the plasma-treated low-κ film against metal diffusion, a 5 nm thick Ta film was sputter deposited on the low-κ films (with and without the 10 s NH_3 plasma treatment at 300°C), followed by the deposition of a 50 nm thick Cu layer. Both metal layers were deposited using a Denton magnetron sputtering system at room temperature. The metallized samples were then subjected to thermal annealing in N_2 at 400°C for 30 min.

Positronium annihilation lifetime spectroscopy (PALS).— PALS measurements were performed at the University of Michigan, Ann Arbor. Details of the PALS apparatus and measurement method have been published elsewhere.[38,39] PALS employs a monoenergetic positron (the anti-particle of an electron) beam to probe porous materials in a high vacuum chamber. Positrons can form positronium (Ps), the bound state of an electron and positron, in materials. Ps tends to trap in electron deficient areas, such as vacancies and voids and the lifetime of the metastable Ps (in vacuum, Ps lives 142 ns) is correlated to the pore size.[40-42] The beam feature of the apparatus allows study of submicrometer thin films. Moreover, the tunable beam energies enable depth profiling, a must for detecting through-thickness film inhomogeneity. Ps makes about one million collisions with the pore wall before annihilation, and probes both closed and open pores. While bouncing off the wall of open pores, Ps can diffuse out of the film through the opening in surface and annihilate in vacuum. The distinctive vacuum Ps lifetime signals the existence of open pores (an "unsealed" surface). On the other hand, the absence of this signal indicates that the pores are either inherently isolated or, in the case of intrinsically interconnected pores, the pore openings near the film surface have been sealed in some
fashion.

For the uncapped pristine LK2200 film, a positron beam of energy ranging from 2.0 to 8.0 keV was implanted into the film. As is discussed later, the pores present in the pristine LK2200 films are highly interconnected and open to the surface. Part of the Ps formed in the film could therefore diffuse out of the film into the vacuum and decay with the vacuum lifetime (142 ns) and thus could not provide pore size information about the film. Hence, for pore size measurement of the pristine LK2200 film, a Si capping layer of 100 nm was sputter deposited onto the dielectric surface to confine Ps to the film, i.e., preventing them from escaping the film. For the capped and plasma treated films, similar measurements were performed using only one or two beam energies.

A further note on the vacuum Ps intensity is necessary to clarify the observed results. Since a low energy positron beam is used to probe the film, there is always a small fraction of incident positrons being reflected back into the vacuum in the state of Ps. Such Ps is called backscattered Ps and added to the data counts with 142 ns lifetime which are due to the escaping Ps from the open pores. The intensity of the backscattered Ps is strongly energy dependent, scaling with the inverse of beam energy, E. The backscattering intensity can be easily calibrated using a dense film or a film with a dense surface, i.e., from which no diffusing Ps escapes. These backscattered Ps are of no interest regarding the pore structure. Therefore, the backscattering intensity was subtracted from the fitted vacuum Ps intensity for the presentation of the results. The vacuum Ps intensity, I_{Vac}, referred to later in the text, included only the escaping Ps.

Nano-indentation measurement.— These experiments were performed at IMRE, Singapore. The elastic modulus and hardness of the thin films were measured using a Nano Indenter XP (MTS Corporation, Nano Instruments Innovation Center, TN) with a continuous stiffness measurement technique at a constant strain rate. The detailed approach has been published elsewhere.[43] An oscillating three-sided pyramid diamond indenter tip (Berkovich) was employed to approach the film surface until contact was detected. The tip was then loaded with a nominal force to advance into the film surface at a constant strain rate of 0.05 s^{-1} to a predetermined depth. The tip was held steady at the maximum depth for 10 s, followed by withdrawal from the sample at the same strain rate as loading. From the load-displacement (P,h) curve, the elastic modulus (E) and hardness (H) are determined using the equations

$$\frac{E}{1-\nu^2} = \frac{\sqrt{\pi}}{2}\frac{1}{\sqrt{A_{max}}}\frac{dP}{dh} \quad [1]$$

and

$$H = \frac{P_{max}}{A_{max}} \quad [2]$$

where A_{max} is the maximum contact area under the maximum indentation load P_{max}, dP/dh is the slope of the indentation unloading curve at P_{max}, and ν is the Poisson's ratio. It has been shown that the Poisson's ratio has little effect on the Young's modulus and hardness values determined using the nano-indentation technique.[44] Consequently, for this study, we choose the Poisson's ratio to be 0.3.

Other measurement and analysis.— The following experiments were also performed at IMRE Singapore. Thicknesses of the LK2200 films before and after plasma treatment were measured using a KLA Tencor Surface Profiler. Before profiling, a U-shaped surface step was created by scratching off the dielectric film using a piece of Si to reveal the flat Si substrate surface of $\sim$50 μm in width. Cross-sectional transmission electron microscopy (XTEM) images were taken with a Philips CM200 FEG microscope. Each cross section TEM sample was prepared by a focused ion beam. A Perkin-Elmer FTIR spectrometer was employed to investigate the bonding structure of the films under the transmission mode. Time-of-flight secondary ion mass spectroscopy (SIMS) was used to analyze the elemental depth profiles of plasma treated films and films subjected to the Ta barrier study. The SIMS depth profile analysis was performed using the CAMECA 6f system under the same analytical conditions for all the samples investigated. A primary O_2^+ ion beam with a net impact energy of 5.5 keV was used.

Results and Discussion

Pristine LK2200 film.— Zirkon LK2200 is a methylsilsesquioxane (MSQ) based porous low-κ film. MSQ is a promising candidate

for ultralow-κ dielectric layers since it has a significantly lower κ value than silicon dioxide, 2.6–2.7 compared to about 4.0.[45] Moreover, due to the methyl groups bonded to the Si–O network of MSQ, it is highly hydrophobic. Acrylic nanoparticles are used as the porogen to introduce about 30% porosity into LK2200 and lower the κ value to 2.2.

To examine the successfulness of pore sealing, the pore structure, especially the pore openness, of the pristine low-κ film needs to be characterized. PALS is a proven technique to examine many aspects of the pore structure in amorphous insulating thin films,[39] such as LK2200. Pore size can be conveniently determined from the Ps lifetime. What is more important is that PALS can quantify the pore openness in terms of pore interconnection length (L_{Int}). In low-κ films such as LK2200, two groups of pores usually coexist. The first group is the sub-nm micropores that exist due to the inefficient packing of the molecules and cross-linked bonding network, and to thermal vibration of chain segments. These micropores are ubiquitous in the film and in the dense version of low-κ materials.[46] These micropores are intrinsic to the material and often neglected in the discussion of pore structures. The second group of pores are the extrinsic pores introduced by high boiling temperature solvents or labile organic pore templates.[6,46] For a low-κ film of a given matrix, such as MSQ, the extrinsic pores dictate the pore structure, the mechanical properties, and other properties related to the porous nature of the film. The extrinsic pores are larger than the intrinsic micropores; the former are often in the range of 2–5 nm in diameter. For convenience in presentation, these extrinsic pores are called mesopores hereafter. When the Ps is located in the mesopores, it is unable to diffuse into the intrinsic micropores because of the associated high energy barrier: the ground state energy of the Ps particle confined in a 2–5 nm diam pore is much lower than its counterpart in a sub-nm pore.[47] Therefore, the diffusion of the Ps in a porous low-κ film is mostly limited to the mesopores in the porous low-κ films, just like the gaseous species during the fabrication process of a microchip. As briefly addressed in the Experimental section, PALS has a unique and convenient ability of depth profiling thin films. When implanted into thin films, the depth distribution of positrons assumes an approximately bell-shaped profile:[48] the positrons roughly spread out over twice the depth of the mean implantation depth, $\bar{Z}$

$$\bar{Z} = \frac{40E^{1.6}}{\rho} \quad [3]$$

where $\bar{Z}$ is in nm, E in keV and density ρ in g/cm^3. Equation 3 is based on a beam whose incident angle is perpendicular to the film surface. In addition, the Michigan positron beam is incident at 45°. Therefore, the equation is modified to

$$\bar{Z} = \frac{40E^{1.6}}{\rho} \times \cos(45°) \approx 28 * E^{1.6} \quad [4]$$

for ρ = 1.0 g/cm^3. The population of Ps formed has a similar profile to the positron implantation profile. However, due to diffusion of the Ps in the interconnected mesopores, Ps can escape out of the film and then be annihilated in vacuum. As can be expected, the fraction of escaping Ps (F_{Esc}) is a function of the positron beam energy. The deeper in the film Ps are formed, the less of them can diffuse out of the film. Therefore, for films with interconnected pores, depth profiling using PALS can quantify the openness of the pores. We define the pore interconnection length (L_{Int}) as the mean depth of positrons at which 50% of the formed Ps in the mesopores escape the film.[49]

PALS is first utilized to characterize the pore structure of the pristine LK2200 film. As shown in Fig. 1a, there are copious vacuum Ps for the film without any plasma treatment or sealing layer, i.e., this film has highly interconnected pores which allowed the implanted Ps to escape back into the vacuum. I_{Vac} decreases from ~20% at 1 and 2 keV to less than 8% at 8 keV. This result is mainly because positrons implanted deeper into the film are expected to have lower probabilities to diffuse out. Besides the vacuum Ps, some fraction of the Ps formed in the mesopores do annihilate in situ. Figure 1b shows the overall Ps intensity formed in mesopores, I_{Meso_All}, including Ps annihilating in both vacuum and mesopores, as a function of E and $\bar{Z}$ for the pristine film and plasma-treated films (at 300°C), respectively. The Ps escape fraction, F_{Esc}, for the pristine film is then calculated as the ratio of I_{Vac} to I_{Meso_All} and plotted in Fig. 1a. Following the definition given in the preceding paragraph, the L_{Int} of the pristine LK 2200 low-κ film is determined to be about 330 nm at 50% F_{Esc}. If the film is isotropic and uniform, this L_{Int} is representative of the length scale over which the pores are interconnected throughout the depth. As shown below, films undergoing plasma treatment are usually inhomogeneous with plasma effect concentrated in the surface region; thus an effective L_{Int} derived in a similar approach no longer represents the characteristic of the pores in the bulk of the film. Considering that the overall thickness of the pristine film is only about 1 μm, L_{Int} at 330 nm means that the mesopores are highly interconnected, or nearing the percolation threshold.

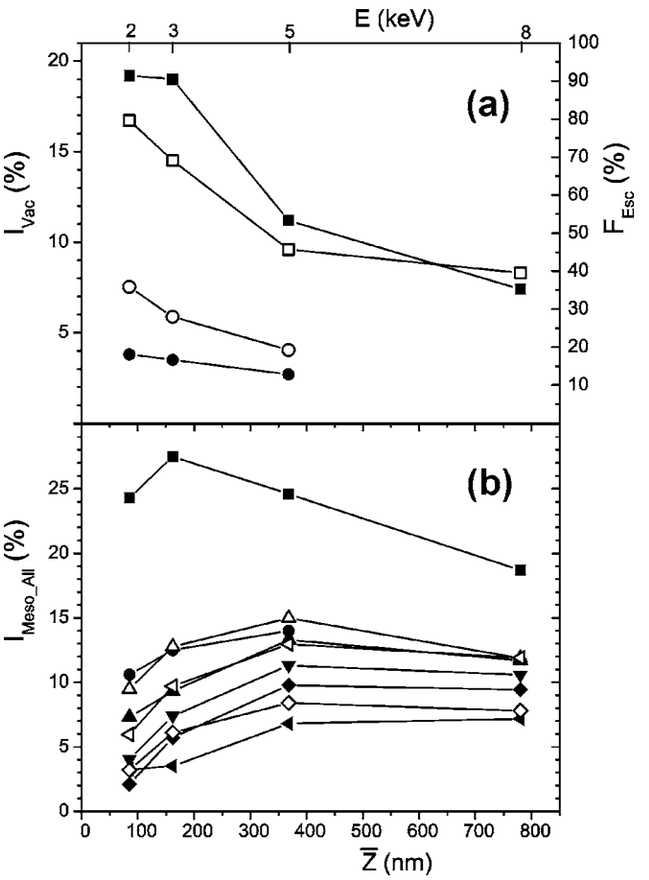

Figure 1. Vacuum Ps intensity, I_{Vac}, [■: pristine; ●: 3 s plasma-treated at 300°C in (a)], Ps escape fraction, F_{Esc}, [□: pristine; ○: 3s plasma-treated at 300°C in (a)], and overall mesopore Ps intensity, I_{Meso_All}, [■: pristine, and plasma-treated at 300°C for 3 s (○), 10 s (▲ △), 30 s (▼), 60 s (◆ ◇), and 600 s (◀ ◁) in (b)] vs positron mean implantation depth $\bar{Z}$ (normalized for density of 1.0 g/cm^3) for LK2200 films. The corresponding positron beam energies, E, for the data points are shown in the top horizontal axis. For the films with plasma-treatment of 10 s, 30 s, 60 s, and 600 s at 300°C, both I_{Vac} and F_{Esc} are zero for all E and therefore not shown.

Since a major fraction of the Ps formed in the mesopores escape the pristine film, the fitted mesopore Ps lifetime is shortened because those Ps that live longer than others tend to diffuse out more readily. In fact, the fitted mesopore Ps lifetime in the pristine film is strongly

dependent on the positron beam energy, or F_{Esc}. The mesopore Ps lifetime increases from 27 to 42 ns as the implantation energy E shifts from 2 to 8 keV and F_{Esc} reduces from 80% to 40%. There may still be some shortening of Ps lifetime at 8 keV with nearly 40% F_{Esc} due to the highly interconnected pores. Therefore, a capping layer on the film surface is required to block the out-diffusion of Ps so that the Ps lifetime thus obtained would be characteristic of the true pore size. For this purpose, a layer of 100 nm Si was deposited on the pristine LKD2200 film by sputtering, and a 49 ± 2 ns Ps lifetime at about 9% was obtained using a positron beam of 8 keV, an energy level sufficient to penetrate the Si capping layer and reach the porous film underneath. Since the mesopores are highly interconnected, a cylindrical pore model[40,42] is appropriate to deduce the pore diameter as 2.7 nm from the Ps lifetime.

NH_3 plasma treatment at 300°C.— From the discussion above, the mesopores in the untreated LK 2200 are highly interconnected and open to the film surface. NH_3 plasma treatment is investigated as a method to seal the film. This particular plasma chemistry is chosen because it has shown promise in low-κ film pore sealing,[27,28] as well as improving copper barrier properties[50] and resistance against moisture uptake and photoresist stripping damage for low-κ materials.[51-54] In most of these cases, the authors concluded that nitride formation played an important role in the improved properties. In the current work, PALS, FTIR, SIMS, TEM, and nanoindentation are used to examine the pore structure change, chemical modification, and other property alteration to the film.

NH_3 plasma treatment at 300°C film temperature is extensively studied. Figure 1a shows the vacuum Ps intensity of the films after exposure to NH_3 plasma at 300°C for a duration of 3–600 s. After plasma exposure of 3 s, the film still has appreciable I_{Vac}, 3–4% at E of 2–5 keV. This I_{Vac} is sharply reduced from that of the pristine film, indicating that the NH_3 plasma is causing pore collapse which blocks some diffusion paths in the surface. Apparently, 3 s plasma exposure at 300°C is not enough to achieve pore sealing and longer exposure time at this temperature is needed. Accompanying the decrease in I_{Vac}, F_{Esc} drops to below 40% even at the lowest E. F_{Esc} does not decrease by the same factor as I_{Vac}, because the overall Ps formation in the mesopores, I_{Meso_All}, also decreases considerably. As shown in Fig. 1b, I_{Meso_All} of the plasma-treated films are significantly less than that of the pristine film. I_{Meso_All} of any plasma-treated films is at most 60% of that of the untreated film. The pristine film forms 25–27% mesopore Ps at E equal to 5 keV and lower. According to Eq. 4, the positron mean implantation depth $\bar{Z}$ is 368 nm at 5 keV, i.e., the bell-shaped positron implantation profile covers almost the full depth of the film. (The density of the pristine film is 0.9 g/cm^3, slightly less than 1.) Therefore it is not surprising to see I_{Meso_All} of the pristine film drop to below 20% at 8 keV, at which $\bar{Z}$ = 780 nm and part of the incident positrons are buried in the underlying Si substrate. The 3 s plasma treated film forms less than 15% mesopore Ps at all beam energies. (The factors causing the reduction in I_{Meso_All} are further discussed in the following paragraph.) The decrease in I_{Meso_All} as well as I_{Vac} was undoubtedly caused by plasma exposure. Although not obvious in the I_{Meso_All} profile for the 3 s treated film, plasma reaction started from the top of the film and will inevitably cause more damage in the surface region. This surface effect is more evident in the films with prolonged plasma exposure, as is addressed in the next paragraph. Therefore, the film after exposure is no longer homogeneous with depth. From the plot of F_{Esc} vs $\bar{Z}$ in Fig. 1a, we can extrapolate that the L_{Int} of the 3 s plasma-treated film is about 50 nm. However, this much smaller L_{Int} is unlikely to represent the pore interconnection length for the film because the pores buried deep in the film, where the NH_3 plasma probably cannot reach, may still have the same L_{Int} as the pristine film at 330 nm. This much shortened "apparent" L_{Int} is simply a measure of the extent of pore collapse.

When we move on to films exposed to plasma longer than 3 s, as noted in the caption of Fig. 1a, I_{Vac} for films treated for 10 s and beyond is zero, i.e., the surface is sealed and no Ps is escaping. This zero value of I_{Vac}, as well as F_{Esc}, serves as a direct and convenient evidence of successful pore sealing. Similar to the 3 s film, I_{Meso_All} of all the plasma treated films, as shown in Fig. 1b, suffer significant decrease in I_{Meso_All}. There is a hint that the loss of I_{Meso_All} is more pronounced for films with longer plasma exposure. Such trend has been reported[37] and also observed in other unpublished work by the Michigan positron group. However, the trend presented in this series in Fig. 1b is far from clear. In fact, the I_{Meso_All} between two films with the same plasma exposure sometimes varies considerably. This is especially true of the 600 s data. As is addressed below, Ps intensity is very sensitive to even slight changes to the film chemistry. I_{Meso_All} of some films might be affected by contact or adsorption of unrelated chemicals during sample handling. In addition, the location of each sample on the original LK2200 wafer surface may also play a role. Regardless, the reduction in I_{Meso_All} by NH_3 plasma exposure is unquestionable. Furthermore, there is a more interesting and important trend of I_{Meso_All} with positron beam energy for all the plasma treated films. As can be seen in Fig. 1b, the reduction in I_{Meso_All} for all the plasma treated films is more drastic at the lowest beam energy, where most positrons stop close to the surface. For the three films with longer plasma exposure, I_{Meso_All} plunges to below 6%, less than one quarter of its counterpart in the pristine film. The sharp decrease of I_{Meso_All} in the surface followed by the strong recovery of I_{Meso_All} as E increases indicates that the plasma damage is concentrated in the upper part or surface region of the film. The argument that the pores deep in the film are left undamaged is supported by the fitted mesopore Ps lifetime in the plasma treated films at about 50 ns, which is consistent with that observed in the Si-capped unprocessed film. This indicates that NH_3 treatment collapses surface pores without affecting the porous structure underneath. As the positron implantation energy increases, more positrons are able to stop in the bulk of the film and form Ps in the mesopores underneath the densified surface region. The combined effects of less Ps formation in the surface layer and penetration of positrons into Si make I_{Meso_All} level off at E above 5 keV, rather than decrease, for the plasma treated films.

Part of the reduction in I_{Meso_All} after plasma treatment can be explained by mesopore collapse caused by plasma exposure. Mesopore collapse should lead to increased Ps annihilation in the MSQ matrix micropores, and indeed we observe this effect: the fitted micropore intensity increases as the fitted mesopore intensity goes down, completely consistent with pore collapse. Unfortunately, the total Ps formation (micropores, mesopores, and vacuum) in the plasma-exposed films is uniformly about 30% less than in the pristine LK2200 film—an effect that cannot be attributed to pore structure in the film. Instead it is most likely due to changes in the chemical environment resulting from the plasma treatment. As is widely observed, the percentage of positrons forming Ps is very sensitive to changes of chemical environment, such as after plasma treatment.[55] Plasma treatment is known to change the chemical composition of the dielectrics,[56,57] and more importantly creating sites of dangling bonds and free radicals that will trap positrons or electrons freed by positrons. The trapping of either positrons or electrons undoubtedly reduces Ps formation.[58] Therefore, the severe reduction of I_{Meso_All} for the plasma treated films, especially at shallow implantation depths, is a combined effect of the mesopore collapse and chemical modification by plasma, which is addressed in the discussion of the SIMS results. Using the observed reduction in the total Ps formation fraction we can reasonably correct the data for the chemical modification effect, thus allowing us to more selectively probe the plasma-induced effects on the pore structure.

The results in Fig. 1, after the correction for chemical-induced changes in the total Ps formation intensity, can then be fitted to a multilayer model of plasma "damage." We find that a simple model of a fully dense layer (complete pore collapse) with layer thickness that increases with plasma exposure time simply does not fit the corrected mesopore intensity data. We obtain a better fit if we use a constant-thickness plasma-modified surface layer around 300 nm

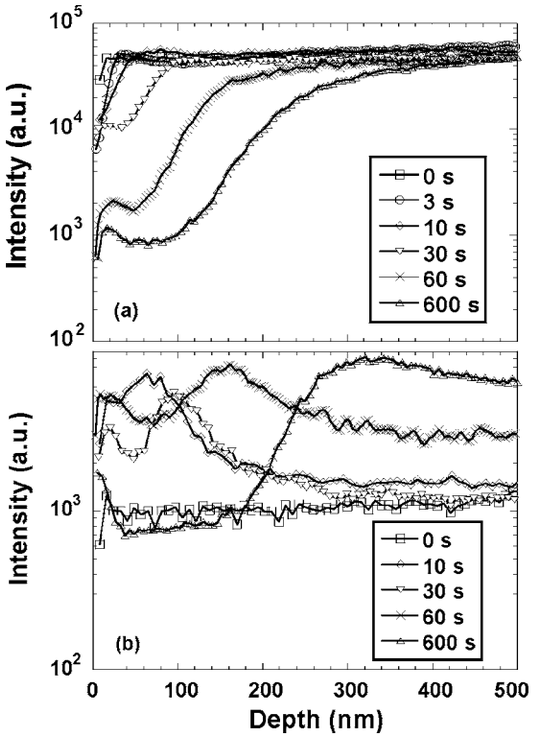

Figure 2. SIMS carbon (a) and nitrogen (b) depth profiles for LK2200 films with varying NH_3 plasma exposure time at 300°C. Note that zero depth corresponds to the new surface of the plasma-treated film. The reduction in film thickness vs plasma exposure time is plotted in Fig. 4.

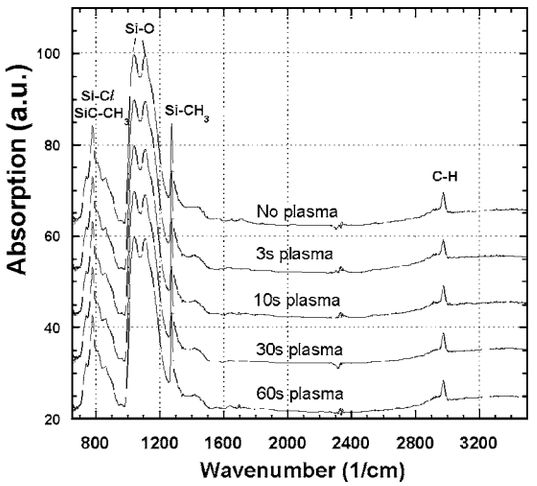

Figure 3. FTIR absorption spectra for LK2200 films after NH_3 plasma treatment at 300°C for different duration.

thick for which the porosity is (for simplicity) nominally constant, but not zero. One can see evidence for this claim in Fig. 1b as all the curves for I_{Meso_All} have roughly the same shape, i.e., the same dependence on depth. They are primarily shifted up and down by some constant intensity corresponding to the Ps plasma-reduced mesopore intensity in this surface layer. One would certainly presume that longer plasma exposure would produce ever lower porosity in the surface layer and the 3 and 10 s exposures do have the highest residual porosity. However, this trend is not perfectly consistent with 30, 60, and 600 s of exposure but the general trend is fairly clear. The pore collapse perpetrated by the plasma extends, not unexpectedly, about the depth over which the pores are inherently interconnected, about 300 nm. The pore collapse is by no means complete over this entire depth; the pore interconnection length may be shorter in length but the pore diameter is unchanged, as evidenced by the steady Ps lifetime with positron beam energy. Despite this fact, all exposure times except the 3 s one produced pore sealing—no Ps was observed to diffuse through the residual porosity. Moreover, the thickness of the dense surface layer as suggested by TEM and nano-indentation measurement is on the order of 10–80 nm for films exposed to NH_3 plasma up to 60 s. About the only way we can reconcile these results is to suggest that the pore collapse in the surface layer is not constant throughout its thickness—that there may be a relatively thin dense layer near the surface that blocks Ps diffusion. Our PALS measurements herein do not have the resolution to probe a 10–20 nm dense layer but the observation of complete pore sealing by plasma exposure at 300°C suggests that there is a dense surface layer that is significantly thinner than the nominal 300 nm depth to which pore collapse extends. We see further evidence for this surface layer in the results from other probes (to be discussed below).

The chemical modification to the dielectric film by the NH_3 plasma is further supported by the SIMS result in Fig. 2. In the untreated film, the Si, C, and O elements are uniformly distributed throughout the film. Compared to the untreated film, one obvious feature in the plasma-treated films is that there is a carbon depletion region on the surface, as shown in Fig. 2a. C depletion has been widely observed in dielectric films exposed to plasma[57] and thus is not further discussed in this paper. In addition to carbon depletion, the concentration of nitrogen (Fig. 2b) is enhanced in the carbon-depleted region, which signals the formation of silicon nitride.[28] It is evident from Fig. 2 that the chemical composition in the carbon depleted region in the surface has changed. Moreover, the C-depleted region grows deeper in the film as the plasma exposure time increases. The C-depletion depth after 3 and 10 s NH_3 plasma treatment is only 30–40 nm. After 30 s, this depth approaches 100 nm, and reaches beyond 150 nm when the exposure time is longer than 60 s. As we have learned from the PALS result, a dense layer is already formed to prevent Ps diffusion back to the vacuum after 10 s plasma exposure. It is tempting to think that the dense layer would serve as a passivation layer and block the plasma from reaching deeper into the film. However, the plasma apparently meets little resistance to push the C-depletion front ever deeper into the dielectric with increasing exposure time. Presumably, plasma generated ions and electrons can still diffuse into the film via the micropores even though most of the mesopores in the surface have collapsed and a continuous path of mesopores through the surface is not available, at least for Ps atoms. In fact, the plasma-induced C-depletion region can reach hundreds of nanometers, even in dense low-κ films,[59] in which only intrinsic micropores exist. For the LK2200 films, such plasma-induced chemistry change is concentrated in the top 150 nm surface layer for less than 60 s plasma exposure, as suggested by the SIMS depth profile result in Fig. 2. The chemistry of the bulk of the film remains little changed, which is further corroborated by the FTIR result in Fig. 3. FTIR is not sensitive to the chemistry change at the film surface; it only shows the bonding structure of the material averaged throughout the film depth. As demonstrated in Fig. 3, no obvious film modification is observed up to 60 s plasma exposure. The absence of obvious bonding structure involving nitrogen in Fig. 3 is attributed, on one side, to poor resolution of such change occurring only in the film surface, and on the other, to convolution of peaks of different bonds, such as Si–C and Si–N in the vicinity of 800 cm^{-1}.

Another indicator of plasma damage is usually obtained through dielectric constant measurements. For example, organosilicate films after severe oxidation by O_2 plasma have been reported to have significantly higher κ value than the untreated film.[52,60] Dielectric constant measurement was attempted on the pristine and plasma-

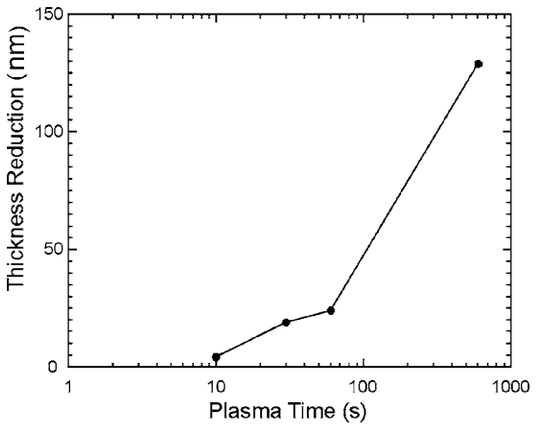

Figure 4. Thickness reduction vs NH_3 plasma exposure time at 300°C for LK2200 films.

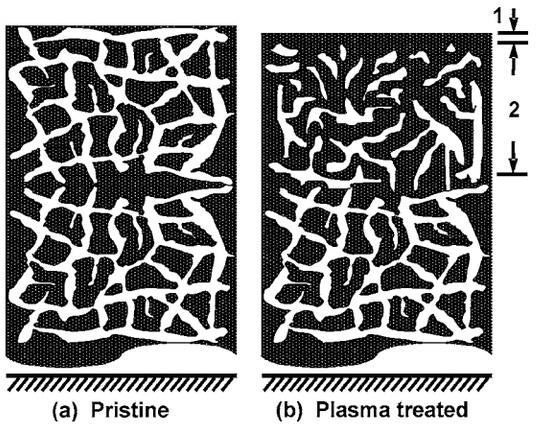

Figure 6. Schematic diagram of LK2200 pore structure before and after plasma treatment. The mesopores in the uniform pristine film interconnect over a length of 330 nm. In the plasma treated films with sealed pores, layer 1 (~10–20 nm thick) is the dense surface layer which blocks Ps diffusion and provides enhanced mechanical properties; layer 2 is a much thicker layer (100–300 nm) influenced by the plasma, where carbon depletion and nitrogen enrichment occur and Ps formation differs from the pristine film.

treated films after depositing round Au dots (1 mm^2 in area and 100 nm in thickness) on top of the dielectric and on the back of the Si wafer. Much higher dielectric constants were unexpectedly obtained on films both before and after plasma treatment. According to the supplier, the dielectric constant of the pristine LK2200 dielectric is 2.2. However, a dielectric constant of 2.55 was calculated from our capacitance-voltage (*C-V*) measurement for the untreated film. This greater value is likely due to the long ambient exposure between dielectric film making and our study. On the other hand, no significant increase of dielectric constant was observed with NH_3 plasma treatment at 300°C for up to 60 s. The 60 s exposure provided a dielectric constant of only 2.64. This small increase of dielectric constant by NH_3 plasma treatment is consistent with findings by other groups. It has been reported that the ammonia plasma treatment increased the dielectric constant of MSQ-type materials by only 0.02 with exposure of less than 10 s.[52,54]

As discussed above, 10 s NH_3 plasma exposure at 300°C achieves the goal in terms of pore sealing. Prolonged plasma exposure undoubtedly poses more pronounced plasma damage, as evidenced by a deeper C-depleted region and more loss in Ps intensity. Film thickness measurement further corroborates this statement. Figure 4 shows the thickness loss due to the etching effect of the ammonia plasma. At 10 s, only ~4 nm of material is removed. If all the reduction in film thickness is due to pore collapse and a fully densified layer is formed in the surface, the thickness of the dense layer is estimated to be 13 nm by assuming that the original porosity is 30%. This is obviously an upper limit of the thickness of a fully dense skin layer since some amount of material is bound to be removed by the ammonia plasma. Nevertheless, this rough estimate is in agreement with the surface layer thickness identified by the XTEM micrograph. As shown in Fig. 5a, the surface of the low-κ film is evidently darkened by plasma treatment, consistent with the formation of a dense skin layer in the surface. The thickness of the darkened layer measured in Fig. 5a is about 10 nm. With extended ammonia plasma exposure duration, thicker skin layers are to be formed accompanied by more loss in film thickness. Figure 5b shows the XTEM micrograph of the film exposed to NH_3 plasma at 300°C for 60 s. A layer of~80 nm of drastically blackened surface layer is evident, and this film is thinned by about 25 nm as shown in Fig. 4. The continuously reduced film thickness through 600 s plasma exposure, at which LK2200 loses nearly 130 nm in thickness, once again demonstrates that the NH_3 plasma does not passivate the film.

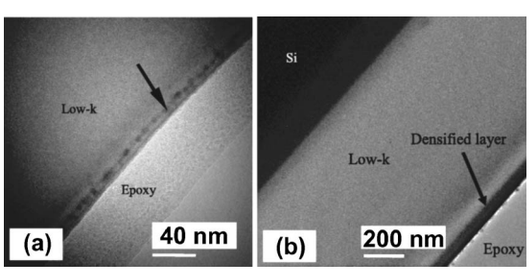

Figure 5. XTEM micrographs of LK2200 films NH_3 plasma treated at 300°C for (a) 10 s and (b) 60 s. Arrows point to the skin layer on the interface between the low-κ film and epoxy.

To summarize the plasma modification to LK2200, we present a schematic drawing of the pore morphology of the dielectric before and after NH_3 plasma pore sealing treatment in Fig. 6. The pristine LK2200 film is presumably uniform and the mesopores are interconnected over a length of 300 nm. After pore sealing, a thin, dense layer is formed at the surface, which confines the Ps in the film. This surface layer is also evident from the TEM micrograph. As will be discussed later, a stiff surface layer is observed in the nanoindentation measurement, most likely due to densification. However, the plasma damage to the film is not limited to the surface region. The PALS results show increased Ps formation in the micropores to a depth of 300 nm indicating some deep-lying pore collapse. This collapse of most likely a small fraction of the pores decreases the apparent pore interconnection length in this layer, but the remaining pores are unaltered in size. Plasma damage over such a depth scale is further corroborated by the SIMS result. C depletion is seen to occur increasingly deeper with longer plasma exposure. Meanwhile, nitrogen enrichment extends at least 200 nm deep into the film. However, the overall plasma damage should remain relatively small, as little adverse effect has been reported on NH_3 plasma treatment of low-κ dielectrics.

Temperature dependence of pore sealing by plasma treatment.— In addition to exposure duration, there are other important factors in plasma treatment that influence, sometimes strongly, the pore sealing process. As we have learned, plasmas alter the dielectric film in more than one aspect. They can densify the surface by collapsing pores, change the film chemistry and bonding structure, and usually remove some material by etching. For a certain plasma chemistry such as NH_3, plasma power, temperature, pressure, flow rate, and other conditions are among parameters that could be controlled. Therefore, a successful plasma pore sealing

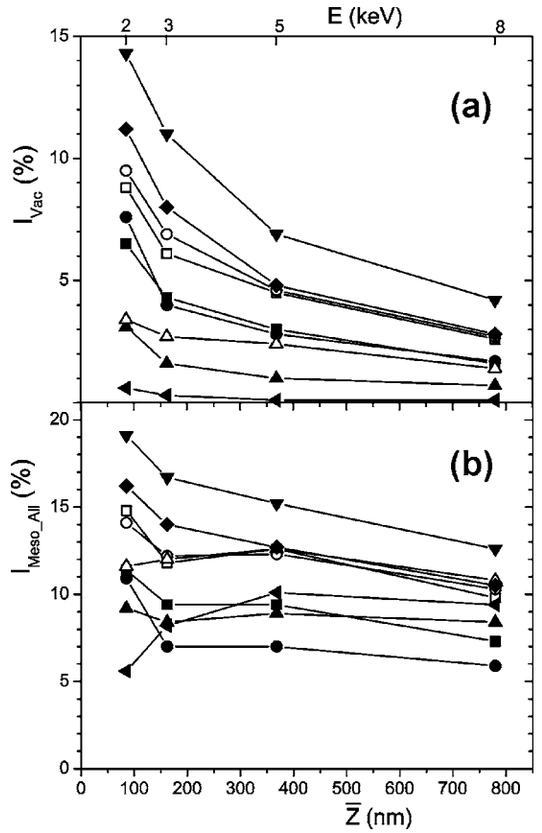

Figure 7. Vacuum Ps intensity (a), I_{Vac}, and overall mesopore Ps intensity (b), I_{Meso_All}, vs positron mean implantation depth $\bar{Z}$ (normalized for density of 1.0 g/cm^3) for plasma-treated LKD2200 films: at 25°C for 3 s (■), 10 s (●), and 60 s (▲); at 100°C for 3 s (□), 10 s (○), and 60 s (△); at 200°C for 3 s (▼), 10 s (◆), and 60 s (◀) The corresponding positron beam energies, E, for the data points are shown in the top horizontal axis.

process needs optimization of these conditions to create a thin dense layer with the least (negative) change to the film chemistry. The optimization process will in return help the understanding of interaction between plasmas and porous dielectrics. However, optimization of every plasma condition is beyond the scope of this collaborative work. In this paper, we focus on the substrate temperature, possibly the most important parameter besides plasma exposure time. The PALS results of treatment at 300°C with varying exposure times has been shown in Fig. 1. The PALS result on NH_3 plasma treatment at 25, 100, and 200°C is organized similarly in Fig. 7.

Figure 7a shows I_{Vac} of films treated at these three lower temperatures for 3, 10, and 60 s, respectively. As stated previously, I_{Vac} is the direct and most convenient indicator of successful pore sealing. To compare with the process at 300°C, we start with the films treated at 200°C. The film treated by 3 s NH_3 plasma at 200°C is nearly as open as the pristine film in terms of the I_{Vac} value. In fact, it is the most open one among all the plasma treated films. In stark contrast, 60 s NH_3 plasma exposure at 200°C leaves the film effectively sealed, with I_{Vac} statistically in agreement with zero. This film is the one closest to pore sealing among all the films presented in Fig. 7. As we focus on Fig. 7b, this film is the only one showing the asymptotic dependence of I_{Meso_All} on positron beam energy, which is characteristic of having a sealed surface as the films in Fig. 1b. Understandably, the result after 10 s treatment at 200°C is in between the previous two, but this 10 s film is still more open than other films treated at lower temperatures. At a substrate temperature of 100°C, 3 and 10 s plasma exposure perform similarly as 10 s treatment at 200°C, while 60 s exposure at 100°C partially sealed

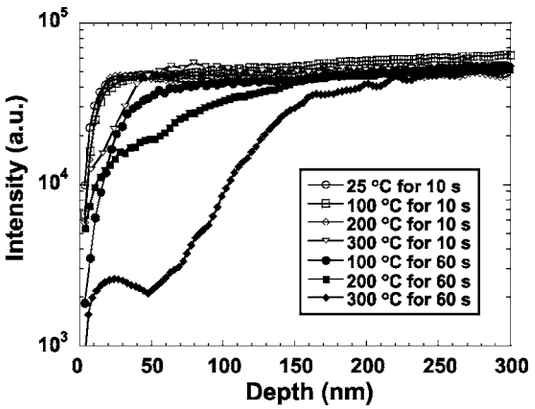

Figure 8. SIMS carbon depth profile for LK2200 after NH_3 plasma exposure at different film temperatures.

the film, lowering I_{Vac} to less than 4% at all positron beam energies. At room temperature, 3 and 10 s exposure also partially seal the film, but 60 s treatment achieves much better results and nearly seals the surface. I_{Vac}, as well as most of the I_{Meso_All} result, decrease with increasing plasma exposure duration at each process temperature, as expected. The detailed comparison among I_{Vac} and I_{Meso_All} of films treated at different temperatures is, however, more complicated and may be beyond simple interpretation. Nonetheless, these data demonstrate that the plasma treatment temperature plays a very important role in the pore sealing process.

At 300°C, the reactivity of the plasma is the highest among all the temperatures investigated; the plasma at this temperature actively induces pore collapse in the surface region of the film and seals the pores. At room temperature and other temperatures, the reactivity of the plasma is lowered, perhaps even significantly. Thus, the plasma damage at these lower temperatures, especially during short exposure, does not cause enough pore collapse to seal off the film surface. In Fig. 8, we show the SIMS carbon depth profile of films after 10 and 60 s plasma treatment at various temperatures. The C-depletion depth after 10 s plasma exposure is more or less independent of the treatment temperature below 200°C. The nominal 20 nm C-depletion depth in contrast to 40 nm for 300°C indicates that the plasma induces less damage to the dielectric at these lower temperatures. The 60 s results clearly demonstrate the temperature dependence of C depletion by NH_3 plasma exposure. For treatment at 100°C, the C-depletion depth is no more than 70 nm after 60 s exposure, while this depth extends beyond 200 nm after treatment at 300°C. Although C depletion is only one aspect of the plasma damages, Fig. 8 convincingly tells us that the plasma reactivity varies strongly with temperature. To cause effective pore sealing during a short treatment, we need the sample temperature to be, e.g., 300°C. Plasma treatment above 300°C might be suggested. It is not a concern here because all the back-end-of-line processes are performed below 350–400°C in consideration of the stability of all the components on microchips.

Improvement of mechanical properties by pore sealing.— It is well established by previous discussion that a dense layer is formed in the surface of the LK2200 film after being exposed to NH_3 plasma at 300°C for as short as 10 s. It will be interesting to observe the effect of the dense layer on the mechanical properties of the dielectric film, e.g., by nano-indentation measurement. Meanwhile, such measurement can provide another estimate of the dense layer thickness as the inhomogenous structure with depth is inevitably reflected in the load-displacement curve.

For a uniform material, the indentation load P is approximately proportional to the square of the displacement h[44]

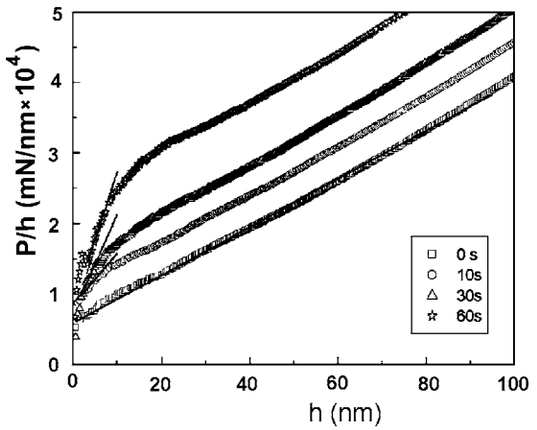

Figure 9. The ratio of indentation load to indentation depth, *P/h*, vs *h* for LK2200 films after NH_3 plasma treatment at 300°C for different durations: 0 s (□), 10 s (○), 30 s (△), and 60 s (☆).

$$P = Ch^2 \quad [5]$$

where *C* is a constant dependent on the properties of the material, such as elastic modulus, yielding stress, and strain hardening. Equation 5 can be rearranged as

$$P/h = Ch \quad [6]$$

Therefore, the plot of *P*/*h* vs *h* is linear for homogenenous materials. This linearity is expected to be observed in the pristine LK2200 film in Fig. 9, for indentation depth up to 100 nm. Generally speaking, nano-indentation measurement on thin films is subjected to substrate influence, especially when the ratio of indentation depth to the film thickness is large. A much stiffer Si substrate underneath the low-κ film will make the curve in Fig. 9 steeper at large *h*. However, this substrate effect is not observed here simply because an indentation depth of 100 nm is relatively small compared to the entire film thickness of ~1.0 μm. On the other hand, the existence of a stiffer surface layer in the plasma treated films is clearly observed in Fig. 9. For the three films treated at 300°C for 10, 30, and 60 s, there is a region below 20 nm where the slope of the curve is larger than that for the bulk of the film. This slope, which is the constant *C* in Eq. 6, reflects the elastic modulus, among other properties, of the material. This means that there is a surface layer of higher modulus in these three films after plasma treatment. As the modulus of porous low-κ materials is closely related to the porosity,[2] it is reasonable to draw the conclusion that a surface layer of enhanced density is formed in these three films. In addition, Fig. 9 once again confirms the assertion that the plasma damage is limited in the surface region of the dielectric film, as the slope of the *P*/*h* curve for the plasma-treated films beyond the surface region is in perfect agreement with that of the pristine film. The depth at the transition point can be used as an estimate of the surface layer thickness. For the three films treated for 10, 30, and 60 s, the dense layer thickness is approximately 7, 10, and 20 nm, respectively. This estimate on the 10 s film is in agreement with what is measured from the XTEM micrograph. Besides the increase of dense layer thickness with plasma exposure time, another clear trend is also demonstrated in Fig. 9. As can be seen, the slope of *P*/*h* vs *h* curve in the surface layer increases with plasma treatment time. That means that the surface layer becomes more and more densified with prolonged plasma exposure, which is consistent with the results obtained by other methods discussed here. The same trend is also demonstrated in the calculated *E* and *H*, as discussed below.

Figure 10 shows the elastic modulus and hardness vs indentation depth for the pristine film and films plasma treated at 300°C for various durations. At any *h*, both *E* and *H* increase with the increase of plasma treatment time, i.e., the mechanical performance is increasingly improved by the formation of an ever denser layer due to ammonia plasma treatment. It would be inviting to determine from Fig. 10 the surface layer modulus and hardness, from which quantitative analysis of the extent of film densification can be drawn. However, the determination of *E* and *H* for the surface layer is very difficult for two reasons. First, the indentation measurement at the very surface is unreliable, as both calculated *E* and *H* decrease significantly at the initial stage of indentation. This "surface effect" is commonly observed in such measurement and stable mechanical properties are usually obtained beyond certain indentation depth. Second, the dense surface layer created in these films is very thin, no more than 20 nm as suggested by Fig. 9. Therefore, the calculated *E* and *H* at any reasonable depth are inevitably coupled with the properties of the undamaged part of the film below the dense surface. It is difficult to extract the mechanical properties of the dense surface layer from Fig. 10, and as the indentation depth increases, the calculated *E* and *H* of the plasma-treated films gradually approximate those of the pristine film. Nonetheless, Fig. 10 clearly shows that the mechanical performance of the dielectric on the whole is improved. Besides simply pore collapse and film densification, another possible reason for improved mechanical properties is silicon nitride formation in the dielectric surface as suggested by the SIMS result in Fig. 2b. Similar improvement in the mechanical properties has also been observed in other NH_3 plasma-treated films.[61] Although the dielectric mechanical performance is more enhanced by longer plasma treatment, such improvement beyond 10 s plasma exposure is offset by aggravated plasma damage as discussed previously.

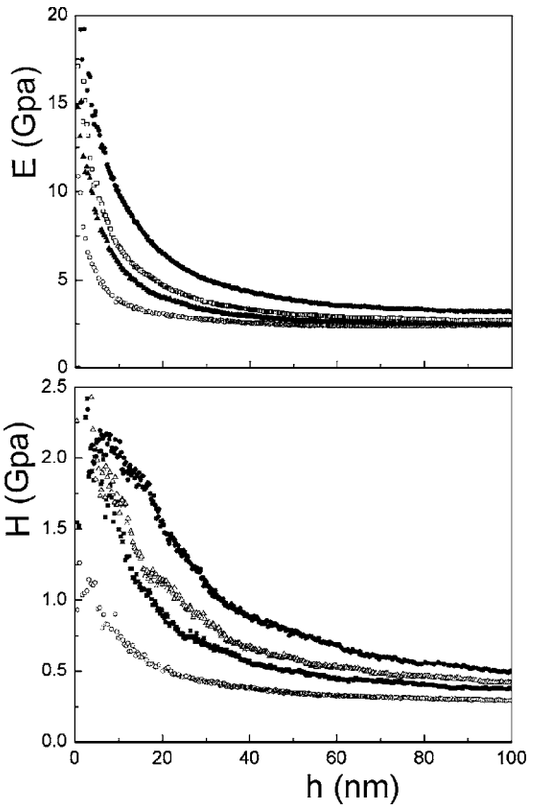

Figure 10. Nanoindentation measurement results on the LK2200 films after NH_3 plasma treatment at 300°C for different durations: elastic modulus (*E*) in the upper panel for 0 s (○), 10 s (▲), 30 s (□), and 60 s (●); hardness (*H*) in the lower panel for 0 s (○), 10 s (■), 30 s (△),and 60 s (●).

Enhanced performance of Ta diffusion barrier due to the presence of plasma-induced dense skin layer.— The performance of thin Ta barrier layer against Cu diffusion at elevated processing

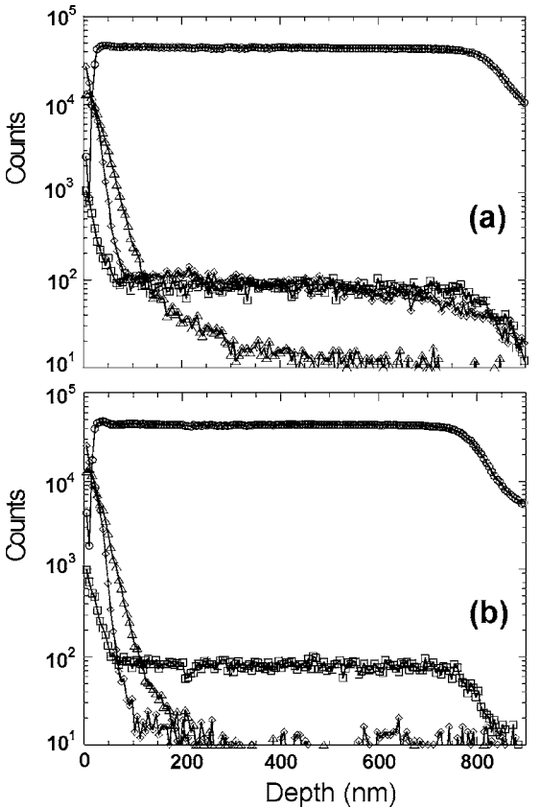

Figure 11. SIMS element depth profile, O (□), Si (○), Cu (◇), and Ta (△) in (a) the pristine LK2200 film, and (b) the plasma treated film at 300°C for 10 s, after the Ta barrier performance test.

temperature is one of the most serious concerns with the integration of porous low-κ in low-κ/Cu interconnect scheme. To evaluate the effect of the plasma-induced dense skin layer on the performance of a thin Ta diffusion barrier, Cu (50 nm)/Ta(5 nm)/Zirkon LK2200 (with and without the 10 s plasma treatment at 300°C) stacks were annealed at 400°C for 30 min. After annealing, the top Cu layer severely agglomerated on the surface so that the film was no longer smooth. To avoid artifacts in SIMS measurement, Cu was selectively removed after annealing using a $(NH_4)_2S_2O_8/H_2O$ solution. SIMS measurement was then taken on the film after Cu removal. The depth profiles of Cu and Ta are shown in Fig. 11a and b. It can be seen from Fig. 11a that a significant penetration/diffusion of Cu through the 5 nm thick Ta barrier layer occurred in the stack formed on the nonplasma treated film after the thermal annealing. There is a Cu plateau at 100 counts extending beyond 600 nm into the dielectric film. In fact, there is also a long Ta tail spreading into LK2200 to a depth of at least 400 nm. In contrast, Ta penetration completely stops at about 200 nm after the films were treated by NH_3 plasma at 300°C for 10 s. More importantly, the penetration/diffusion of Cu through the Ta barrier layer was drastically reduced, or even completed suppressed; Cu is effectively absent beyond a sputtering depth of 100 nm. The poor performance of the 5 nm thick Ta on nonplasma treated film is most likely due to the reduction of the effective thickness of the Ta layer and/or the presence of pinholes in the thin Ta layer due to the substantial diffusion of Ta into underlying porous low κ. The sealing of surface pores by NH_3 plasma treatment and the consequently formed nitride dense skin layer would, on the other hand, promote the formation of a continuous Ta barrier free of pinholes and other defects accessible for Cu diffusion. Therefore, the thin Ta barrier remained as an effective diffusion barrier against Cu penetration during subsequent thermal annealing at 400°C.

Conclusion

It has been demonstrated in this paper that NH_3 plasma treatment is a viable approach to achieving pore sealing in porous low dielectric constant films. Plasma-induced pore collapse and chemical modification can extend to a film depth that is consistent with the mean pore interconnection length (here ~300 nm). More importantly, by controlling the treatment temperature and duration, it is possible to concomitantly form a much thinner (10–20 nm) dense layer that seals the pore openings at the surface with relatively inconsequential damage to the remaining dielectric. This thin dense layer also tends to improve both the mechanical properties of the dielectric film and the performance of Ta barriers in preventing Cu diffusion.

Acknowledgments

The authors thank the University of Michigan, Ann Arbor, the Institute for Materials Research and Engineering, Singapore, and National Science Foundation (no. ECS-0100009) for supporting this research.

References

1. W. W. Lee and P. S. Ho, *MRS Bull.*, **22**, 19 (1997).
2. K. Maex, M. R. Baklanov, D. Shamiryan, F. Iacopi, S. H. Brongersma, and Z. S. Yanovitskaya, *J. Appl. Phys.*, **93**, 8793 (2003).
3. A. Grill, V. Patel, K. P. Rodbell, E. Huang, M. R. Baklanov, K. P. Mogilnikov, M. Toney, and H. C. Kim, *J. Appl. Phys.*, **94**, 3427 (2003).
4. A. Grill and D. A. Neumayer, *J. Appl. Phys.*, **94**, 6697 (2003).
5. Q. G. Wu and K. K. Gleason, *J. Vac. Sci. Technol. A*, **21**, 388 (2003).
6. J. L. Hedrick, R. D. Miller, C. J. Hawker, K. R. Carter, W. Volksen, D. Y. Yoon, and M. Trollsas, *Adv. Mater. (Weinheim, Ger.)*, **10**, 1049 (1998).
7. S. Yang, P. A. Mirau, C. S. Pai, O. Nalamasu, E. Reichmanis, J. C. Pai, Y. S. Obeng, J. Seputro, E. K. Lin, H. J. Lee, J. N. Sun, and D. W. Gidley, *Chem. Mater.*, **14**, 369 (2002).
8. J. H. Yim, M. R. Baklanov, D. W. Gidley, H. Peng, H. D. Jeong, and L. S. Pu, *J. Phys. Chem. B*, **108**, 8953 (2004).
9. M. Fayolle, G. Passemard, O. Louveau, F. Fusalba, and J. Cluzel, *Microelectron. Eng.*, **70**, 255 (2003).
10. R. Hoofman, G. Verheijden, J. Michelon, F. Iacopi, Y. Travaly, M. R. Baklanov, Z. Tokei, and G. P. Beyer, *Microelectron. Eng.*, **80**, 337 (2005).
11. E. T. Ryan, J. Martin, K. Junker, J. Wetzel, D. W. Gidley, and J. N. Sun, *J. Mater. Res.*, **16**, 3335 (2001).
12. S. M. Rossnagel, A. Sherman, and F. Turner, *J. Vac. Sci. Technol. B*, **18**, 2016 (2000).
13. H. Kim, *J. Vac. Sci. Technol. B*, **21**, 2231 (2003).
14. H. Kim, *Surf. Coat. Technol.*, **200**, 3104 (2006).
15. D. Edelstein, C. Uzoh, C. Cabral, P. DeHaven, P. Buchwalter, A. Simon, E. Cooney, S. Malhotra, D. Klaus, H. Rathore, B. Agarwala, and D. Nguyen, in *Proceedings of the IEEE 2001 International Interconnect Technology Conference*, June 4–6, 2001, p. 9 (2001).
16. G. Beyer, A. Satta, J. Schuhmacher, K. Maex, W. Besling, O. Kilpela, H. Sprey, and G. Tempel, *Microelectron. Eng.*, **64**, 233 (2002).
17. W. Besling, A. S. Satta, J. Schuhmacher, T. Abell, V. Sutcliffe, A. M. Hoyas, G. Beyer, D. Gravesteijn, and K. Maex, in *Proceedings of the IEEE 2002 International Interconnect Technology Conference*, June 3–5, 2002, p. 288 (2002).
18. S. G. Lee, Y. J. Kim, S. P. Lee, H. S. Oh, S. J. Lee, M. Kim, I. G. Kim, J. H. Kim, H. J. Shin, J. G. Hong, H. D. Lee, and H. K. Kang, *Jpn. J. Appl. Phys., Part 1*, **40**, 2663 (2001).
19. Y. W. Koh, K. P. Loh, L. Rong, A. T. S. Wee, L. Huang, and J. Sudijono, *J. Appl. Phys.*, **93**, 1241 (2003).
20. V. Jousseaume, M. Fayolle, C. Guedj, P. H. Haumesser, C. Huguet, F. Pierre, R. Pantel, H. Feldis, and G. Passemard, *J. Electrochem. Soc.*, **152**, F156 (2005).
21. C. M. Whelan, Q. T. Le, F. Cecchet, A. Satta, J. J. Pireaux, P. Rudolf, and K. Maex, *Electrochem. Solid-State Lett.*, **7**, F8 (2004).
22. J. S. Juneja, G. A. Ten Eyck, H. Bakhru, and T. M. Lu, *J. Vac. Sci. Technol. B*, **23**, 2232 (2005).
23. C. Jezewski, C. J. Wiegand, D. X. Ye, A. Mallikarjunan, D. L. Liu, C. M. Jin, W. A. Lanford, G. C. Wang, J. J. Senkevich, and T. M. Lu, *J. Electrochem. Soc.*, **151**, F157 (2004).
24. P. de Rouffignac, Z. W. Li, and R. G. Gordon, *Electrochem. Solid-State Lett.*, **7**, G306 (2004).
25. T. Abell and K. Maex, *Microelectron. Eng.*, **76**, 16 (2004).
26. A. M. Hoyas, J. Schuhmacher, C. M. Whelan, J. P. Celis, and K. Maex, *Microelectron. Eng.*, **76**, 32 (2004).
27. X. T. Chen, D. Gui, D. Z. Chi, W. D. Wang, N. Babu, N. Hwang, G. Q. Lo, R. Kumar, N. Balasubramanian, and D. L. Kwong, *IEEE Electron Device Lett.*, **26**, 616 (2005).

28. X. T. Chen, D. Gui, Z. Q. Mo, A. Y. Du, D. Z. Chi, W. D. Wang, Y. H. Wang, D. Lu, L. J. Tang, W. H. Li, and L. Y. Wong, *Thin Solid Films*, **504**, 248 (2006).
29. G. Mannaert, M. R. Baklanov, Q. T. Le, Y. Travaly, W. Boullart, S. Vanhaelemeersch, and A. M. Jonas, *J. Vac. Sci. Technol. B*, **23**, 2198 (2005).
30. W. J. Cho, R. Saxena, O. Rodriguez, M. Ojha, R. Achanta, J. L. Plawsky, and W. N. Gill, *J. Electrochem. Soc.*, **152**, F61 (2005).
31. N. Posseme, T. David, T. Chevolleau, and O. Joubert, *Electrochem. Solid-State Lett.*, **8**, G112 (2005).
32. S. Takeishi, H. Kudoh, R. Shinohara, A. Tsukune, Y. Satoh, H. Harada, and M. Yamada, *J. Electrochem. Soc.*, **143**, 381 (1996).
33. T. C. Chang, P. T. Liu, Y. S. Mor, S. M. Sze, Y. L. Yang, M. S. Feng, F. M. Pan, B. T. Dai, and C. Y. Chang, *J. Electrochem. Soc.*, **146**, 3802 (1999).
34. H. R. Kim, H. H. Park, S. H. Hyun, and G. Y. Yeom, *Thin Solid Films*, **332**, 444 (1998).
35. P. T. Liu, T. C. Chang, S. M. Sze, F. M. Pan, Y. J. Mei, W. F. Wu, M. S. Tsai, B. T. Dai, C. Y. Chang, F. Y. Shih, and H. D. Huang, *Thin Solid Films*, **332**, 345 (1998).
36. A. M. Hoyas, J. Schuhmacher, C. M. Whelan, M. R. Baklanov, L. Carbonell, J. P. Celis, and K. Maex, *J. Vac. Sci. Technol. B*, **23**, 1551 (2005).
37. J. N. Sun, D. W. Gidley, Y. Hu, W. E. Frieze, and E. T. Ryan, *Appl. Phys. Lett.*, **81**, 1447 (2002).
38. J. N. Sun, D. W. Gidley, Y. F. Hu, W. E. Frieze, and S. Yang, in *Mater. Res. Soc. Symp. Proc.*, **726**, Q10.5.1 (2002).
39. D. W. Gidley, H. G. Peng, and R. S. Vallery, *Annu. Rev. Mater. Res.*, **36**, 49 (2006).
40. D. W. Gidley, W. E. Frieze, T. L. Dull, A. F. Yee, E. T. Ryan, and H. M. Ho, *Phys. Rev. B*, **60**, R5157 (1999).
41. T. L. Dull, W. E. Frieze, D. W. Gidley, J. N. Sun, and A. F. Yee, *J. Phys. Chem. B*, **105**, 4657 (2001).
42. D. W. Gidley, W. E. Frieze, T. L. Dull, J. Sun, A. F. Yee, C. V. Nguyen, and D. Y. Yoon, *Appl. Phys. Lett.*, **76**, 1282 (2000).
43. L. Shen, K. Y. Zeng, Y. H. Wang, B. Narayanan, and R. Kumar, *Microelectron. Eng.*, **70**, 115 (2003).
44. P. L. Larsson, A. E. Giannakopoulos, E. Soderlund, D. J. Rowcliffe, and R. Vestergaard, *Int. J. Solids Struct.*, **33**, 221 (1996).
45. J. H. Yim, Y. Y. Lyu, H. D. Jeong, S. K. Mah, J. Hyeon-Lee, J. H. Hahn, G. S. Kim, S. Chang, and J. G. Park, *J. Appl. Polym. Sci.*, **90**, 626 (2003).
46. J. H. Yim, M. R. Baklanov, D. W. Gidley, H. G. Peng, H. D. Jeong, and L. S. Pu, *J. Phys. Chem. B*, **108**, 8953 (2004).
47. K. P. Mogilnikov, M. R. Baklanov, D. Shamiryan, and M. P. Petkov, *Jpn. J. Appl. Phys., Part 1*, **43**, 247 (2004).
48. P. J. Schultz and K. G. Lynn, *Rev. Mod. Phys.*, **60**, 701 (1988).
49. H. G. Peng, R. S. Vallery, M. Liu, W. E. Frieze, D. W. Gidley, J. H. Yim, H. D. Jeong, and J. Kim, *Appl. Phys. Lett.*, **87**, 161903 (2005).
50. Y. Shioya, T. Ishimaru, H. Ikakura, Y. Nishimoto, T. Ohdaira, R. Suzuki, and K. Maeda, *J. Electrochem. Soc.*, **151**, C56 (2004).
51. Y. J. Mei, T. C. Chang, S. J. Chang, F. M. Pan, M. S. K. Chen, A. Tuan, S. Chou, and C. Y. Chang, *Thin Solid Films*, **308**, 501 (1997).
52. P. T. Liu, T. C. Chang, H. Su, Y. S. Mor, Y. L. Yang, H. Chung, J. Hou, and S. M. Sze, *J. Electrochem. Soc.*, **148**, F30 (2001).
53. K. M. Chang, I. C. Deng, S. J. Yeh, and Y. P. Tsai, *Electrochem. Solid-State Lett.*, **2**, 634 (1999).
54. T. C. Chang, Y. S. Mor, P. T. Liu, T. M. Tsai, C. W. Chen, Y. J. Mei, and S. M. Sze, *Thin Solid Films*, **398**, 632 (2001).
55. D. L. Moore, R. J. Carter, H. Cui, P. Burke, S. Q. Gu, H. G. Peng, R. S. Valley, D. W. Gidley, C. Waldfried, and O. Escorcia, *J. Electrochem. Soc.*, **152**, G528 (2005).
56. K. Yonekura, S. Sakamori, K. Goto, M. Matsuura, N. Fujiwara, and M. Yoneda, *J. Vac. Sci. Technol. B*, **22**, 548 (2004).
57. H. Cui, R. J. Carter, D. L. Moore, H. G. Peng, D. W. Gidley, and P. A. Burke, *J. Appl. Phys.*, **97**, 113302 (2005).
58. D. M. Schrader and Y. C. Jean, *Positron and Positronium Chemistry*, Elsevier, New York (1988).
59. Y. H. Wang, R. Kumar, X. Zhou, J. S. Pan, and J. W. Chai, *Thin Solid Films*, **473**, 132 (2005).
60. Y. S. Mor, T. C. Chang, P. T. Liu, T. M. Tsai, C. W. Chen, S. T. Yan, C. J. Chu, W. F. Wu, F. M. Pan, W. Lur, and S. M. Sze, *J. Vac. Sci. Technol. B*, **20**, 1334 (2002).
61. S. Kim, Y. Toivola, R. F. Cook, K. Char, S. H. Chu, J. K. Lee, D. Y. Yoon, and H. W. Rhee, *J. Electrochem. Soc.*, **151**, F37 (2004).